Adaptive and Space-Filling Peptide Self-Assembly Upon Drying

Dhwanit R. Dave[1,2,3,#], Salma Kassem[1,#], Maeva Coste[1,#], Mona Tayarani-Najjaran[1,2,3,#], Lele Xu[1,4], Sheng Zhang[1], Darjan Podbevsek[1,5], Luis Ortuno Macias[5], Deborah Sementa[1], Muniyat A. Choudhury[1,6], Kelly Veerasammy[1,8], Selma Doganata[1,6], Cory Weng [1,6], Jorge Morales[7], Tong Wang[1], Mateusz Marianski[2,3,9], Tai-De Li[1,10], Xi Chen[1,2,5,11], Raymond Tu[5], Ye He[1,4,*] and Rein V. Ulijn[1,2,3,9,*]

1. Advanced Science Research Center (ASRC), The Graduate Center of the City University of New York, 85 St. Nicholas Terrace, New York, NY 10031 (USA)
2. Ph.D. Program in Chemistry, The Graduate Center of the City University of New York, 365 Fifth Avenue, New York, NY 10016 (USA)
3. Department of Chemistry, Hunter College, City University of New York, 695 Park Avenue, New York, NY 10065 (USA)
4. Ph.D. Program in Biology, The Graduate Center of the City University of New York, 365 Fifth Avenue, New York, NY 10016 (USA)
5. Department of Chemical Engineering, The City College of New York, New York, NY, 10031 (USA)
6. Macaulay Honors College, City University of New York, New York, NY, 10031 (USA)
7. Department of Biology, City College of New York, New York, NY, 10031 (USA)
8. SUNY Downstate Medical Center, Brooklyn, NY 11203, (USA)
9. Ph.D. Program in Biochemistry, The Graduate Center of the City University of New York, 365 Fifth Avenue, New York, NY 10016 (USA)
10. Department of Physics, City College of New York, City University of New York, New York, NY 10031, (USA)
11. Ph.D. Program in Physics, The Graduate Center of the City University of New York, 365 Fifth Avenue, New York, NY 10016 (USA)

Abstract: Peptides have tremendous potential as building blocks of designer materials with wide-ranging applications. These materials are stabilized by strongly directional hydrogen bonding patterns giving rise to one-, or two-dimensional assembly. It remains a challenge to mimic biology's context-adaptive and flexible structures. Here, we introduce minimalistic tripeptide sequences that form dynamic ensembles through incorporation of multivalent sidechain interactions that collectively self-optimize depending on their context. Notably, we observed that these dispersions undergo drying-induced liquid to solid phase separation involving interface stabilization and expansion, resulting in formation of films of stiff, and densely packed, porous peptide microparticles that can be instantaneously redispersed upon re-introduction of water. Air-drying of aqueous peptide dispersions in the presence of proteins or small molecule payloads results in spontaneous and efficient encapsulation, and retention of protein stability after redispersion. These supramolecular tripeptide dispersions show promise for emulsification, encapsulation, and storage of biomacromolecules.

Introduction

All life forms share conserved sets of building blocks. Biomolecular covalent and non-covalent interactions dictate the rich structural design space, supporting wide-ranging functions, including recognition, self-assembly, catalysis, shape-shifting. Beyond their critical roles in the chemistry of life, these structures provide inspiration for supramolecular materials[1–4] and systems[5] for (bio-)technological applications[6] and more.[7,8]

Peptide materials usually contain patterns of backbone hydrogen-bonding derived from protein secondary structures,[9–13] typically giving rise to one-dimensional (1D)[14,15] or two-dimensional (2D) structures.[16,17] These H-bond patterns may be further stabilized by aromatic stacking,[18] giving rise to architectures that are remarkably stiff and stable.[19] This is exemplified by 'dry' diphenylalanine (FF) zippers[20,21] that have remarkable mechanical, optical and electronic properties.[7] We previously established that aromatic tripeptides with polar groups, such as lysine-tyrosine-phenylalanine (KYF), retain strong directional self-assembly tendencies complemented with favorable solvent interactions, leading to hydrogelation. [22–24]

Besides 1D and 2D structures, the notion of non-directional assembly is also common in biology, *e.g.*, in liquid condensates[15,25] typically leading to spherical morphologies dictated by surface tension. In these systems, side-chain interactions dictate the assembly complementing flexible backbone interactions.[26-27] Short peptide motifs that display liquid-liquid phase separation have been reported,[28,27] including through flexible linkers separating aromatic dipeptides to disrupt directionality.[29]

Beyond structures with intrinsic (non-) directionality through backbone or side-chain interactions, biology frequently employs architectures that display structural agility in response to external factors. This may be achieved through dynamic selection and adjustment from the complex side-chain interaction space available. This concept has been demonstrated in synthetic systems, where the adaptive versatility of biomimetic random heteropolymer sequences with flexible backbones and multiple (randomized) functional sidechain have been shown to adaptively decorate and wrap proteins[30], or recapitulate dynamic features of protein ensembles in biofluids.[31]

Here, we introduce sequence designs of tripeptides that are not isotropic through backbone H-bonding interactions, but instead form dynamic ensembles through multiple possible combinations of weak and reversible interactions, by combining polar, H-bonding aromatic and basic residues (tryptophan, tyrosine, lysine, W/Y/K) (Figure 1a) (Figure 1b). We show that these peptides form aqueous dispersions (Figure 1c) with unique properties, including formation of mechanically stiff particles that instantaneously redisperse, and the ability to wrap, encapsulate and stabilize proteins.

Results

Directionality and dispersibility in peptide self-assembly: sidechain *vs* backbone interactions

We reasoned that systematically modulating aromatic interaction strength and directionality through variation of side-chains (F, Y, W) could lead to motifs with richer and dynamic sidechain interactions (Figure 1a, b). Indeed, it has been observed that exchanging F or Y for tryptophan (W) removes the strong directionality from minimalistic self-assembling peptide systems.[27,32-33] Compared to phenylalanine, tryptophan's non-covalent interaction space is expanded to include not only $\pi - \pi$, cation-π, but also H-bonding (distinct from tyrosine due to the indole NH), NH-π and dipole-dipole interactions, importantly, including with water (Figure 1a).[34,35] It is worth noting that tryptophan supports precise roles in proteins enabled by its unique heteroaromatic nature, such as specific interfacial functions in proteins, *e.g.,* near lipid bilayers and ion channels.[35,36] Thus, we first examined the self-assembling behavior of KFF, KYF, KYY, KYW, known to aggregate based on coarse-grained molecular dynamics (MD) simulations.[24]

We used atomistic MD simulations to reveal differences in molecular interactions (Figure 1b, d, Figure S11). First, exchanging F→Y→W leads to an increase in the aggregation propensity (AP) (Figure 1d, Supplemental Figures S12). We analyzed the contribution of the backbone-backbone (as a proxy for 1D self-assembly), backbone-sidechain, and sidechain-sidechain hydrogen bonds (Figure 1d, Supplemental Figures S13-16). Consistent with the increased AP scores, we observed a concomitant increase in the total number of hydrogen bonds in F→Y→W variants. Of these hydrogen bonds, backbone-backbone interactions decreased, while participation of the sidechain-backbone and sidechain-sidechain hydrogen bonds increased in the Y and W containing sequences (Figure 1d). The data show that the introduction of H-bonding capabilities from the rotationally flexible sidechains can favor non-directional assembly, especially for KYW (Figure 1d).

The relative contributions of sidechains and backbone interactions when substituting F→Y→W are also evident in the circular dichroism (CD) spectra (Figure 1e). At a concentration of 5 mM, which is just above the critical aggregation for KYF and KYY show a carbonyl $\pi \rightarrow \pi^*$ transition peak at 203 nm which is a consequence of backbone-backbone interactions (Supplemental Figures S17a-c). For KYW, this transition is less intense, while the appearance of the 229 nm positive signal confirms the dominating influence of tryptophan sidechains interactions.[37] We also monitored the CD for the three tripeptides (KYF, KYY and KYW) at concentrations ranging from 0.5 mM up to respectively 10, 5 or 20 mM (Supplemental Figures S18a-c). KYF and KYY eventually undergo gelation and phase separation, but KYW remarkably retains the appearance of a clear solution up to 20 mM (Figure 1c). The CD data was in agreement with previously reported characterization using TEM, where KFF, KYF and KYY images show nanoscale fibers whereas KYW displayed amorphous aggregates (Supplemental Figure S19, Figure S20 shows formation of soluble aggregates by DLS)[24]. Thus, while KFF, KYF, KYY show directional assembly because of backbone H-bonds, KYW forms soluble ensembles that are stabilized by dynamic side chain

interactions. No evidence of phase separation was observed by microscopy, indicating that these ensembles are dynamic and have less defined boundaries.

Sequence-dependence in tripeptide dispersions

We previously demonstrated differential assembly of tripeptide sequence isomers driven by side-chain induced conformation selection.[23] We speculated that in a system that is stabilized by a multitude of possible side-chain and water interactions, these would not be defined by one dominant conformation, but instead represented by an ensemble of conformers. We studied the six K/Y/W sequence isomers to determine the sequence-dependent self-assembly (Figure 1f, Supplemental Figure S21-26) and found comparable AP scores (Figure 1f, Supplemental Figure S21) and similar ratios of sidechain/backbone interactions (Figure 1f, Supplemental Figure S22-25), consistent with formation of non-directional ensembles. We also analyzed the solvent exposure of tryptophan, measured through Solvent-Accessible Surface Area (SASA) (Figure 1f, Supplemental Figure S26) of the indole sidechain. This was found to be sequence-dependent, with WYK and WKY the most contrasting in terms of AP and tryptophan solvent exposure (Figure 1g).

Tryptophan exposure in peptide ensembles could be experimentally verified by measuring the tryptophan emission, which is widely used as a probe to detect the tryptophans' environment and solvent exposure in proteins,[48-53] with red-shifted emissions indicating an increase in local polarity and blue-shifts indicating hydrophobic environments.[38–42] These ensembles (20 mM) did not show evidence of phase separation when observed by optical microscopy, and they displayed a faint blue emission under UV light (shown for KYW in Figure 1c). We measured the emission spectra of all sequence isomers in soluble dispersions (Figure 1h) and found that emission maxima (λ_{ex} = 280 nm) range from 357 nm to 370 nm with the most red-shifted emission corresponding to the most hydrated tryptophan (WYK) and the most blue-shifted emission corresponding to the most hydrophobic tryptophan environment (WKY) (Figure 1g). The 3D excitation/emission spectra of contrasting sequences (Figure 1h) differed by the appearance of a new band in WYK's spectrum at λ_{ex} = 318 nm, which is also prominent in YKW and YWK. We also found that the intensity and absence/presence of the band is concentration dependent, suggesting its origin from an emissive state of a supramolecular arrangement (Supplemental Figure 27a-b).

In order to verify the existence of dynamic, but discrete ensembles, the contrasting sequences WKY and WYK were analyzed by DLS, and we observed similar diameter sizes (450-500 nm size range) but with a distinct narrower size dispersion for WYK (Supplemental Figure S20). To further confirm differential environments experienced by tryptophans, the ^{1}H-NMR spectra of WYK and WKY solutions at variable concentrations show contrasting concentration-dependent chemical shifts of W protons (Supplemental Figure S28). The indole ring protons in WYK shift downfield as the concentration increases from 1 to 5 to 20 mM indicating their positioning in an electron poor environment and formation of a polar network/hydrogen bonding while (minimal) upfield shifts were observed for WKY, in line with the formation of π-π stacking driven aggregation.

Evaporation-driven assembly

Upon investigation of the fluorescence of KYW peptide assemblies using confocal microscopy, to our surprise we observed a remarkable phase separation behavior that was triggered by localized evaporation during drying. Given the important (competing) role of water in modulating interactions in these dynamic ensembles, in particular those involving tryptophan, the observation led us to study assembly during gradual removal of water through evaporation of sessile droplets (Figure 2a).[43-44]

Macroscopically, when observing tripeptide assembly in drying droplets starting from 20 mM peptide dispersions, we observed surprising contrasting behaviors. A strongly scattering ring upon drying for KYW in contrast to KFF, KYF, and KYY that give rise to heterogeneous semi-transparent structures (Figure 2b, Supplemental Videos 1-2). When observed by microscopy (Figure 2c, Supplemental Figure S29), the differential morphologies (1D fibers versus 3D spherical objects) are evident (Supplemental Figure S30 showing KFF and KYF). When observed over time, KYW displays a remarkable interfacial phase separation behavior, giving rise to formation of films composed of densely packed spherical particles (Figure 2d, Supplemental Video 3), contrasting KFF, KYF, KYY that give rise to 1D structures with varying degrees of bundling, resembling previous observations for evaporation-driven assembly of peptide derivatives (Supplemental Figure S29, Supplemental Videos 4-6).[45] We propose that the multitude of possible interactions and the flexibility of the backbone enable the K/Y/W peptides to more effectively reconfigure and adapt to the newly formed interfaces that form upon water evaporation. The observed (lack of) directionality initiates at the molecular level, and clearly translates hierarchically to macroscopic scales. We observe complex drying patterns, related to solvent and solute gradients in drying of droplets,[46] with phase separation occurring at the drying front due to concentration gradients inside the drying droplet.

Based on previously reported interfacial supramolecular aggregation of tripeptides in oil/water emulsions,[46] we hypothesized that the sequence-dependent tryptophan exposure in ensembles would lead to interfacial aggregation and reduction in surface tension. We measured the dynamic tension profile *via* the pendant drop method[47] of tripeptides WYK, WKY, and KYW, which have contrasting W solvent-exposure and environments. We found that surface adsorption of peptide ensembles reduced surface tension correlating with W-solvent exposure (sequence dependence) (Supplemental Figure S31), demonstrating that the peptide ensembles dynamically interact at the air/water interface.

Despite these differences in collective conformations and sequence-dependent W exposure both in solution and at interfaces, upon drying inside droplets we observed that each of the sequences gave rise to similar sequential phase separation behavior, forming droplets followed by solidification to form solid particle films, similar to KYW (Figure 2e, Supplemental Figure S32). Upon analysis of the tryptophan emission in the dried films at 5% relative humidity (RH), we note

a general loss of emission from the 318 nm band in the 3D excitation/emission spectra with spectra of the dried films now suggesting a redistribution of conformations (Figure 2e, Supplemental Figure S33). The original variable W exposure was in part recovered by temporarily exposing the solid film to high humidity (95% RH). These data highlight the adaptive nature of the assemblies where tryptophan partitioning reversibly changes depending on competing water via weak multivalent interactions.

Formation of buoyant droplets and porous particles

Upon microscopy analysis of the dried particulate films, we observed the expected spherical objects, but also porous, disk-shaped particles of varying sizes with flat surfaces (Figure 3a.i). These structures are found at the top of the sample (Figure 3b-c, Supplemental Figure S34), suggesting that they are formed at the air-water interface. The observation suggests that, in contrast to typical dense coacervate droplets that sediment, the structures studied here are low-density, buoyant condensates. The observation of flattened 2D hemi-spherical objects suggests that these particles are initially liquid and due to their low density, they rise to the interface, where they deform, flatten, and solidify. This observation is confirmed using FIB SEM (Figure 3c), which shows a part-circular cross-section. The pore size distribution ranged from 30-500 nm (Supplemental Figure S35).

We propose that the observed buoyancy is related to the formation of gas bubbles inside liquid droplets (Figure 3a.i). This may be a consequence of a secondary phase separation event where the condensate interface nucleates gas bubble formation, which is stabilized by adherence of indoles to gas/aqueous interfaces (Figure 3a.ii). Notably, degassing of the peptide dispersion prior to evaporation-driven assembly lead to smaller particles of more spherical morphology (Figure 4e). This observation indicates that the buoyant nature of the droplets relates to their gas content, and it can be regulated. Non-surface particles are smaller and spherical, indicating fusion and flattening at the air-water interface (Figure 3b). TEM analysis of glutaraldehyde crosslinked KWY particles reveals highly and fine porous and spherical structure of the non-surface particles (Figure 3c-d). The hemispherical porous structure was further confirmed by AFM (Figure 3e). Young's Modulus analysis demonstrated that these particles are mechanically stiff (6 GPa) due to the efficient and packing (Figure 3f) in line with previously reported FF derivatives[21].

Size control, reversibility, and drying-induced encapsulation

We propose that the spontaneous formation of tightly packed particles upon air drying — could be useful in emulsification, encapsulation and drying strategies that do not rely on input of strong mechanical forces. We first investigated whether the size distribution of the particles formed could be controlled. Given the important role of water evaporation in this process, we reasoned that by simply increasing the temperature, evaporation will occur faster, and consequently, the formation of solid particles is accelerated. We observed that temperature increase gives rise to a more homogeneous and smaller particles (Figure 4a-b, Supplemental Figure S36a-b). The combination

of reduced buoyancy, due to lower gas content at elevated temperature, with acceleration of phase transition and solidification, yields particles that are monodisperse (Supplemental Figure S36c-e).

As an alternative method to control particle size, we removed the air from the solution through sonication under vacuum followed by storage under argon gas and examined the drying process in a degassed solution under argon. Live confocal time-lapse imaging of the particle forming process revealed smaller droplets (Supplemental Figure S37a). Further Imaris 3D reconstruction and analysis demonstrated a 20-fold reduction in particle volume and increase in sphericity in the degassed samples compared to prevalence of disk-shaped particles non-degassed samples (Figure 4c-e, Supplemental Videos 7-8). Consistent with the role of air in pore formation, degassed peptide particles show fewer and smaller pores (Supplemental Figure S37b).

Next, we probed the reversibility of the process. Upon re-introduction of 5 µl droplet of water on top of a dried film, the structures immediately re-dispersed as shown in Figure 4f. When this droplet was left to dry again, the particle film reappeared after a few minutes, demonstrating that the process is fully reversible (Supplemental Video 9). These observations strongly contrast previously reported peptide materials, where formation of 1D and 2D structures are highly stable due to large enthalpic gain from cooperative H-bonds which are not readily reversed. Peptide ensembles with multivalent, weak, and dynamic interactions offer more reversible assemblies as water solvation can compete with the energetics of the interaction space.

We proceeded to test whether the approach could be potentially useful for encapsulation. We used the small organic fluorophore Alexa 488, which has been previously demonstrated to non-covalently conjugate through the sulfonate group and lysine side chains.[48] Upon introduction of the dye, it is encapsulated during droplet formation and solidification (Supplemental Figure S38, Supplemental Video 10). Analysis of the fluorescence intensity of the pre-load mixture of peptides and dye, the formed liquid droplets, and the post-load solution, revealed highly efficient enrichment of dye inside particles (Supplemental Figure S38b).

Next, inspired by the ability of dynamic interacting polymers with random distributions of side chain functionalities to stabilize proteins through adaptive of matching of side chain interactions to complementary patches on the protein surface[30,49], we investigated the ability to encapsulate and stabilize Enhanced Green Fluorescent Protein (EGFP). We observed efficient encapsulation inside the structures for the dynamically assembling peptide, WKY (Figure 4g-h, Supplemental Figure S39). As EGFP fluorescence requires a folded conformation, we evaluated the preservation of structure in the dried state (Figure 4i-j, Supplemental Video 11). After drying and subsequent rehydrating the EGFP solution loses its fluorescence (Figure 4k-l), whereas WKY+EGFP sample shows retention of fluorescence emission after drying, storage in dried form for five days, followed by instantaneous re-dissolution. The control KYF+EGFP (fibrous assembly) reveals a decrease in the fluorescence suggesting a level of stabilization through protein/peptide interactions. These results highlight that the drying peptide ensembles provide an environment where proteins are

stabilized, including in the dried state, possibly through mechanisms analogous to dynamic interfacial complexation through self-organization of side chains with protein surface (Figure 4j).[49] These data suggests that K/Y/W isomer tripeptides offer potential as minimalistic modalities for encapsulation, drying, storage, and redispersion of proteins.

Conclusions

Introduction of combinations of side chains able that cover a rich interaction space in self-assembling tripeptides enables context-adaptive assembly. Through air-drying, dynamically assembly tripeptides give rise to spontaneous formation of high-porosity solids upon water evaporation that are instantaneously redispersed. The observed assembly and phase behavior is governed by side chain interactions in contrast to rigid hydrogen-bond patterns that typically dictate 1D or 2D architectures in self-assembling molecules. MD simulations and fluorescence data collectively demonstrate that the six sequence isomers of K/W/Y form soluble ensembles with the sequence dictating the preferred interactions, but upon drying-induced assembly, all sequences give rise to particle films with comparable emission in the dried state, suggesting that regardless of sequence tryptophan plays comparable stabilizing interactions. The phase separation process enables encapsulation of small molecule and protein payloads, and they are rapidly and fully reversible upon re-introduction of water. We propose that this peptide-based evaporation-driven emulsification and encapsulation approach, combined without mechanical energy input may find applications in storage and formulation of biomacromolecules.

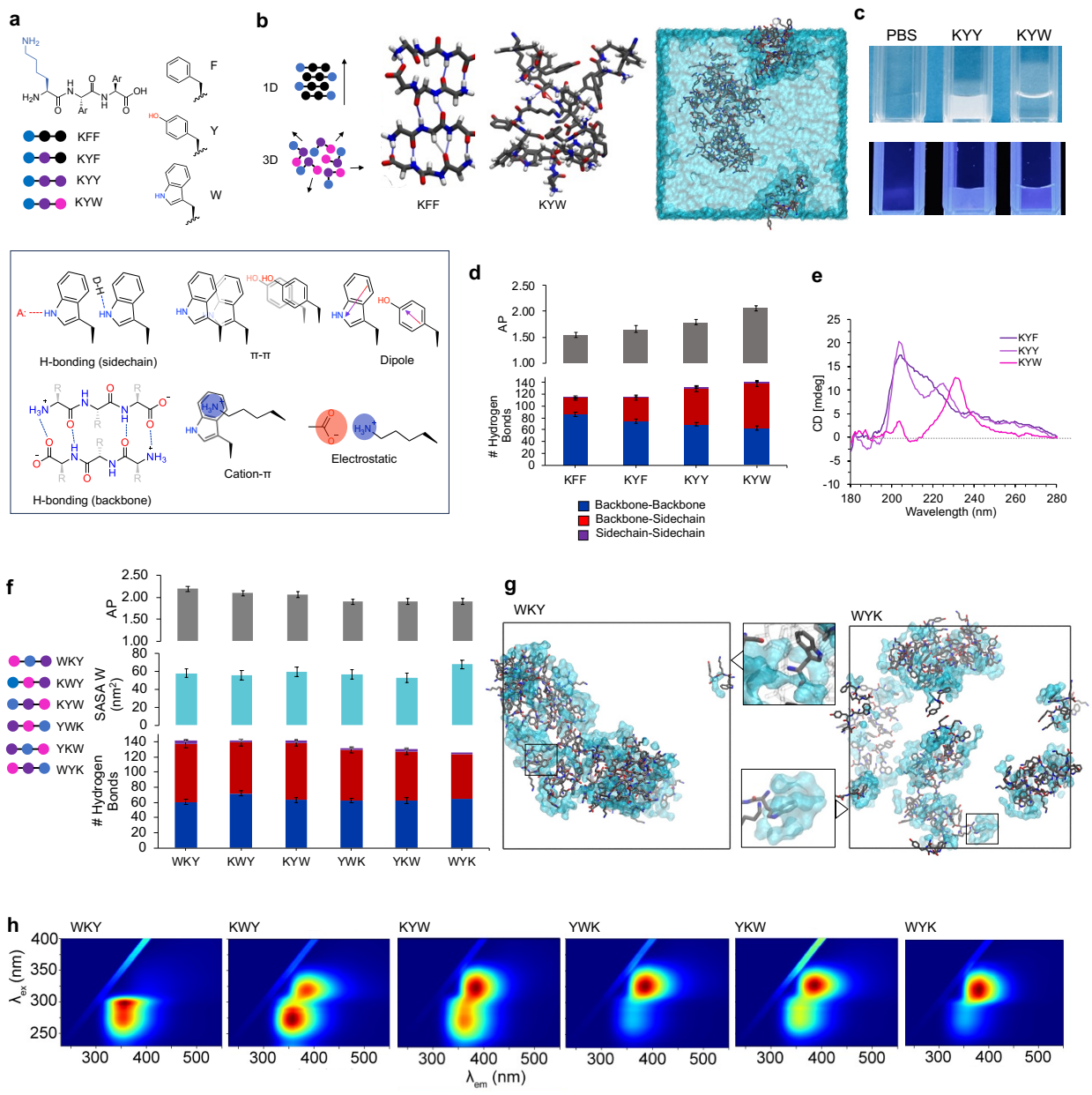

Figure 1. Directionality in peptide self-assembly. a. Chemical structures of tripeptides KFF, KYF, KYY, KYW and representation of the interaction space of sidechains. b. Selected snapshots of simulations for KFF (only backbone shown for clarity) and KYW, with predominant H-bond interactions highlighted. c. (Left) Macroscopic images of the materials formed by the indicated tripeptides (20 mM in phosphate buffer at pH 7), under visible light (top) or UV light (bottom). Phosphate buffer (PBS) was used as a control. (Right) Snapshot from MD trajectory of KYW showing assembly inside a water box. d. (Top) Sequence-dependent aggregation propensity, AP=($SASA_{initial}/SASA_{last50ns}$) and (Bottom) distribution of hydrogen bond interactions between simulated peptides from MD trajectories. Backbone and sidechain as an indication of directionality of self-assembly. Averages and s.d. error bars from 3 replicate trajectories e. Circular Dichroism spectra of KYF, KYY and KYW measured at 5 mM concentration at pH 7.5. f. AP score, W Solvent accessible surface area (SASA) and hydrogen bonding interaction distribution analyses for K/Y/W sequence isomer MD trajectories. Averages and s.d. error bars from 3 replicate trajectories g. Snapshots for WKY and WYK showing non-directional self-assembly resulting in differential tryptophan environments and water binding (shown in

blue) with zoomed areas showing a dry (top) and water bound (bottom) tryptophan. h. 3D fluorescence spectra showing the differential polarity and water-interactions of tryptophan residues in solution.

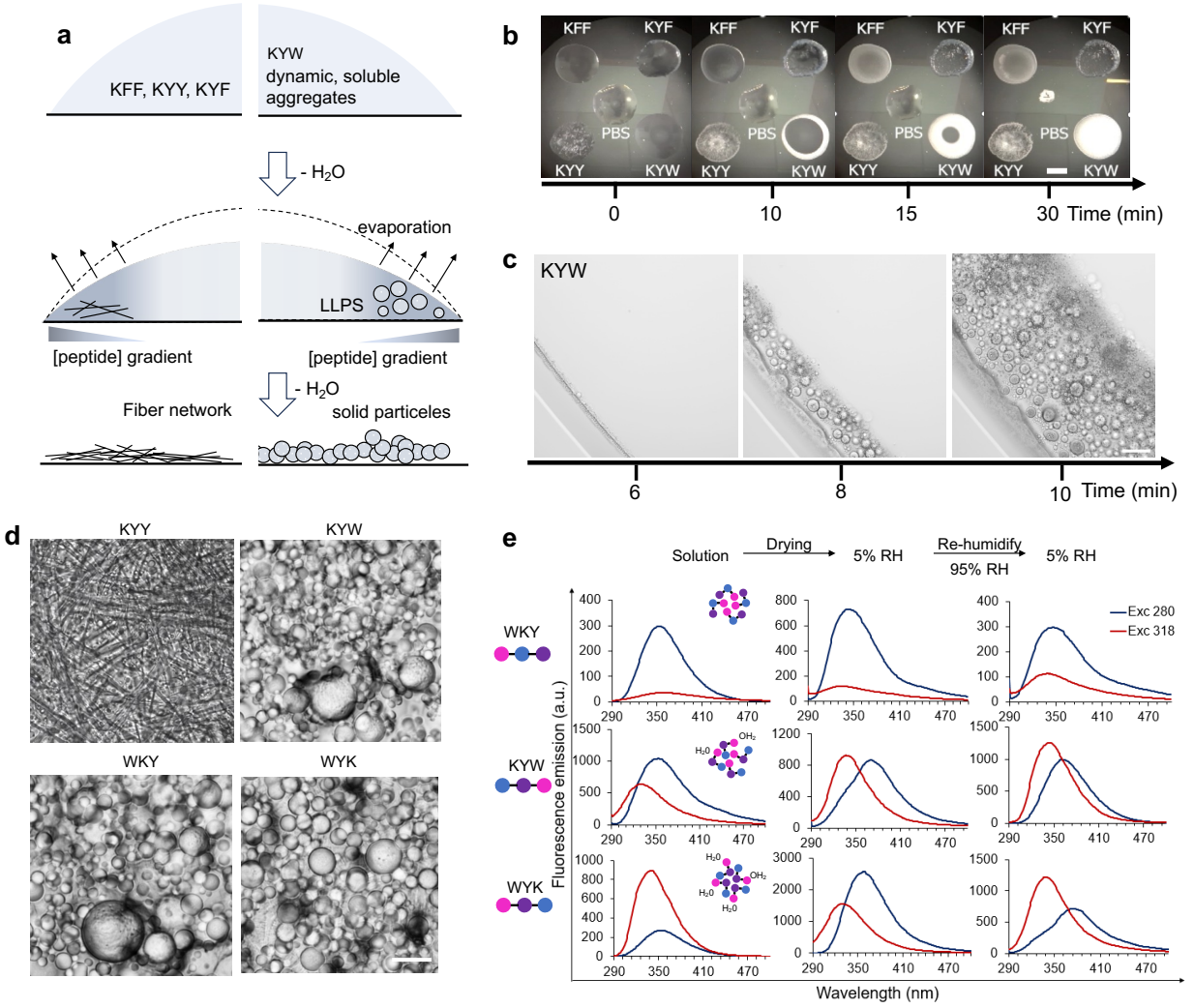

Figure 2. Sequence-dependance in evaporation-driven assembly. a. Representation of evaporation-driven self-assembly in sessile droplets. b. Evaporation patterns over time with differential assembly of KYW clearly visible. Scale bar = 1 mm. c. Microscopy time course for evaporation-driven assembly of KYW. Scale bar = 50 µm d. Final optical microscopy image showing 1D assembly for KYY) and space-filling assemblies for KYW, WKY and WYK (left) (right). Scale bar = 10 µm. e. Fluorescence emission spectra at two different excitation wavelength (280 and 318 nm) of the different sequences in solution, dried foams (visual appearance shown in d) and rehydrated foams reveals similar packing in dried particle film, suggesting comparable evaporation-driven assembly regardless of sequence and recovery of sequence dependent conformation selection in hydrated state.

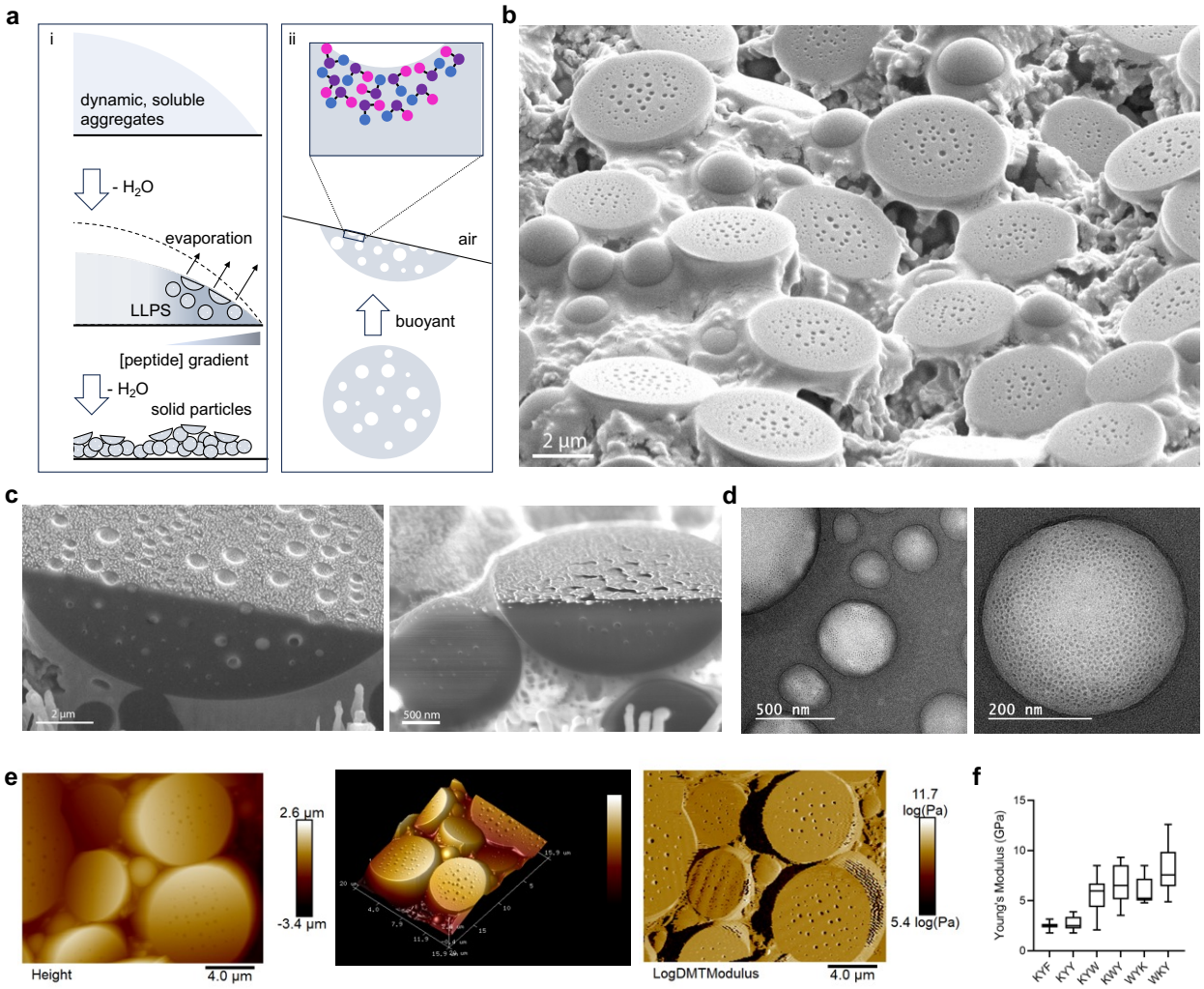

Figure 3. Formation of porous particles and half-domes during evaporation-driven tripeptide assembly. a. Schematic representation of evaporation-driven assembly of buoyant liquid droplets that settle at the droplet interface and upon drying form half-dome shaped particles. Images of KWY dried foam b. SEM image showing half-dome particles at the interface and also showing surface pores. c. FIB-SEM analysis confirming half-dome shape and revealing the porous structure inside of foam particles. Note that the fine granular structures on the surface are from sputtered-coated gold. e. TEM analysis of glutaraldehyde crosslinked KWY dissociated particles reveals that non-surface particles are highly porous spheres. e. AFM analysis showing porous half-dome particles. f. The plot of Young's Modulus stiffness of fibers or particles formed by indicated peptides. Total 15-36 particles or fibers were profiled for each sequence.

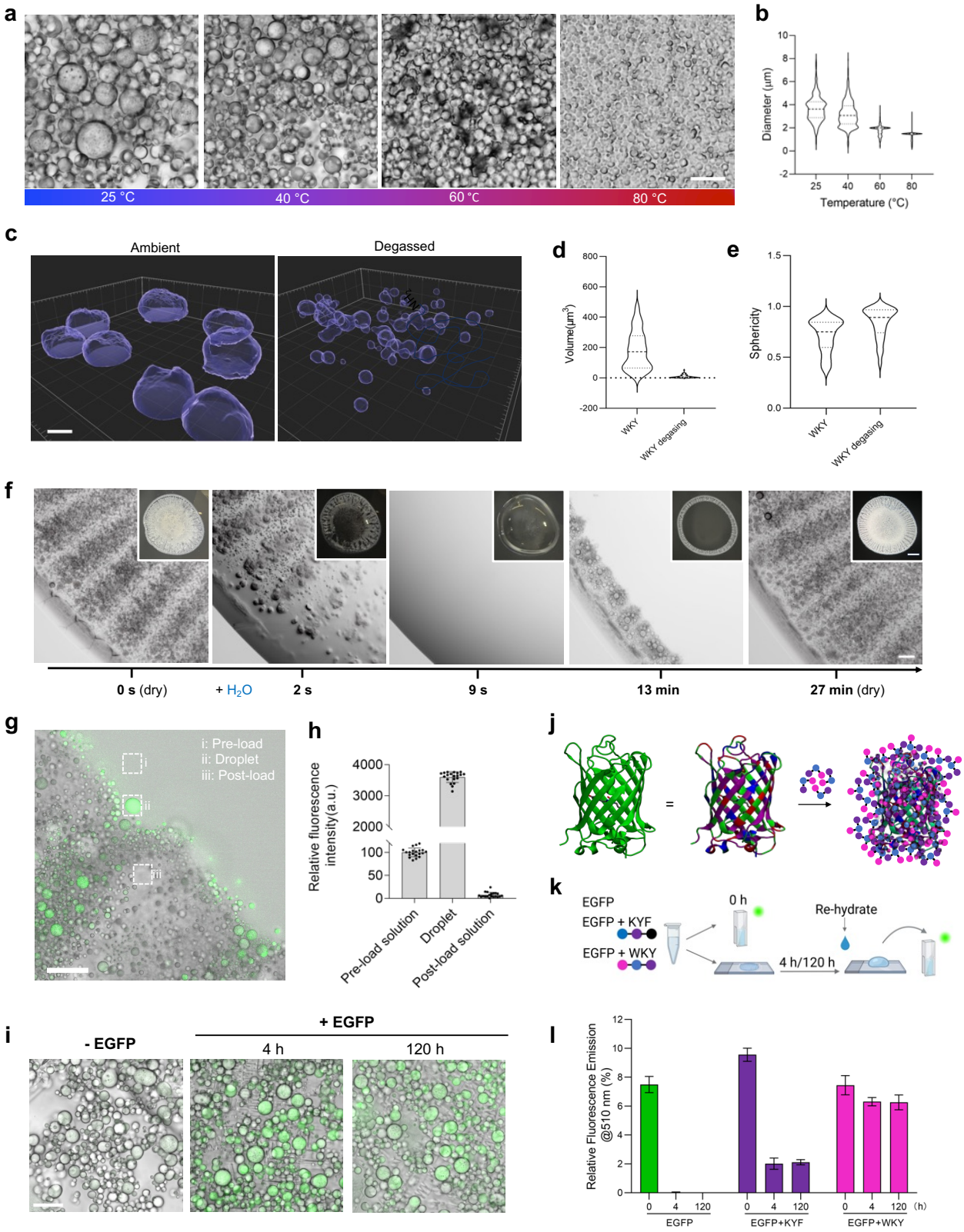

Figure 4. Evaporation-driven emulsification and encapsulation in dynamic peptide ensembles. a-b. Temperature dictates the size distribution of particle films. The example of KWY shows reduction in particle size and more homogeneous size distribution, which correlated with the increased temperature during evaporation. Scale bar = 10

μm. Total 368 - 1456 particles at each temperature were analyzed. c. The peptide solution was degassed followed by evaporation assay, and the example of WKY is shown. Imaris 3D rendering demonstrated reduction in particle size and increase in sphericity as plotted in d and e respectively. Scale bar = 5 μm. f. Fully reversible formation of porous peptide foams upon addition of water and re-evaporation. Representative time-lapse images of KWY were shown. Scale bar = 50 μm. The macroscopic images of 5 μl peptide solution drop at each stage were shown in the insertion. g. Confocal live imaging of KWY peptide particles incorporating EGFP shows significant enrichment of EGFP protein in peptide droplets. Scale bar = 20 μm. h, Fluorescence intensity analysis of the pre-load solution, the droplet, and the post-load solution at the frontier of emulsification. A total of 20 regions of each indicated groups from 6 time-lapse frames were quantified, and the average intensity of pre-load solution was set as 100 arbitrarily. Error bar represents s.d. i. Confocal and bright field imaging of dried peptide particles reveal that the green fluorescence signals of EGFP retain in WKY peptide particles under ambient condition for 5 days after solidification. j. Schematic showing EGFP protein with residue nature color coded and potential interactions with peptides during encapsulation. k-l. Experiment to test the storage and re-dispersion ability of WKY with a schematic representation of the experiment and the fluorescence emission at 510 nm (λexc. = 488 nm) of the corresponding solution (EGFP, EGFP+KYF and EGFP+WKY) over time. Error bars represent s.d. from 3 replicate experiments.

Acknowledgment

R.V.U., D.D., M.C. acknowledge funding from Office of Naval Research for the Vannevar Bush Faculty Fellowship (Grant No. N00014-21-1-2967). We thank the Air Force Office of Scientific Research for funding of R.V.U., D.S., S.K. (Grant No. FA9550-21-1-0091). NMR data presented herein were collected at the City University of New York, Advanced Science Research Center (CUNY ASRC) Biomolecular NMR Facility by James Aramini. The TFA removal protocol has been provided by Dr. Gary Scott. The imaging experiments were carried out in the Live Imaging and Bioenergetics Core, Surface Science Core, and Imaging Suite at ASRC. Y.H. and T.W. are supported by PSC-CUNY Faculty Research Award jointly funded by the Professional Staff Congress and The City University of New York. M.A.C. and S.D. were supported by Velay Women Scholarship and K. V. was supported by Sloan Foundation CSURP program. T.L. acknowledges support through NIH 1S10OD030401-01A1.

1. Aida, T., Meijer, E. W. & Stupp, S. I. Functional Supramolecular Polymers. Science. 335, 813–818 (2012).

2. Zhang, S. Fabrication of novel biomaterials through molecular self-assembly. Nat. Biotechnol. 21, 1171–1178 (2003).

3. Ghadiri, M. R., Granja, J. R., Milligan, R. A., McRee, D. E. & Khazanovich, N. Correction: Self-assembling organic nanotubes based on a cyclic peptide architecture. Nature. 366, 324-327 (1993).

4. Freeman, R. et al. Reversible self-assembly of superstructured networks. Science. 362, 808–813 (2018).

5. Sheehan, F. et al. Peptide-Based Supramolecular Systems Chemistry. Chem. Rev. 121,

13869–13914 (2021).

6. Du, X., Zhou, J., Shi, J. & Xu, B. Supramolecular Hydrogelators and Hydrogels: From Soft Matter to Molecular Biomaterials. Chem. Rev. 115, 13165–13307 (2015).

7. Tao, K., Makam, P., Aizen, R. & Gazit, E. Self-assembling peptide semiconductors. Science. 358, (2017).

8. Sinha, N. J., Langenstein, M. G., Pochan, D. J., Kloxin, C. J. & Saven, J. G. Peptide Design and Self-assembly into Targeted Nanostructure and Functional Materials. Chem. Rev. 121, 13915–13935 (2021).

9. Levin, A. et al. Biomimetic peptide self-assembly for functional materials. Nat. Rev. Chem. 4, 615–634 (2020).

10. Woolfson, D. N. A Brief History of De Novo Protein Design: Minimal, Rational, and Computational: De novo protein design. J. Mol. Biol. 433, 167160 (2021).

11. DeGrado, W. F. & Korendovych, I. V. De novo protein design, a retrospective. Q. Rev. Biophys. 53, e3 (2020).

12. Hulgan, S. A. H. & Hartgerink, J. D. Recent Advances in Collagen Mimetic Peptide Structure and Design. Biomacromolecules 23, 1475–1489 (2022).

13. Omenetto, F. G. & Kaplan, D. L. New opportunities for an ancient material. Science. 329, 528–531 (2010).

14. Yuan, C. et al. Hierarchically oriented organization in supramolecular peptide crystals. Nat. Rev. Chem. 3, 567–588 (2019).

15. Perry, S. L. Phase separation: Bridging polymer physics and biology. Curr. Opin. Colloid Interface Sci. 39, 86–97 (2019).

16. Gallego, L., Woods, J. F. & Rickhaus, M. Recent Concepts for Supramolecular 2D Materials. Org. Mater. 4, 137–145 (2022).

17. Magnotti, E. L. et al. Self-Assembly of an α - Helical Peptide into a Crystalline Two-Dimensional Nanoporous Framework. Journal of the American Chemical Society. 138, 16274-16282 (2016).

18. Reches, M. & Gazit, E. Casting metal nanowires within discrete self-assembled peptide nanotubes. Science. 300, 625–627 (2003).

19. Chakraborty, P. et al. Co-Assembly between Fmoc Diphenylalanine and Diphenylalanine

within a 3D Fibrous Viscous Network Confers Atypical Curvature and Branching. Angew. Chemie 132, 23939–23947 (2020).

20. Azuri, I., Adler-Abramovich, L., Gazit, E., Hod, O. & Kronik, L. Why are diphenylalanine-based peptide nanostructures so rigid? Insights from first principles calculations. J. Am. Chem. Soc. 136, 963–969 (2014).

21. Bera, S. et al. Rigid helical-like assemblies from a self-aggregating tripeptide. Nat. Mater. 18, 503–509 (2019).

22. Piotrowska, R. et al. Mechanistic insights of evaporation-induced actuation in supramolecular crystals. Nat. Mater. 20, 403–409 (2021).

23. Lampel, A. et al. Polymeric peptide pigments with sequence-encoded properties. Science. 356, 1064–1068 (2017).

24. Frederix, P. W. J. M. et al. Exploring the sequence space for (tri-)peptide self-assembly to design and discover new hydrogels. Nat. Chem. 7, 30–37 (2015).

25. Gebbie, M. A. et al. Tuning underwater adhesion with cation-φ interactions. Nat. Chem. 9, 473–479 (2017).

26. Abbas, M., Lipiński, W. P., Wang, J. & Spruijt, E. Peptide-based coacervates as biomimetic protocells. Chem. Soc. Rev. 50, 3690–3705 (2021).

27. Leshem, A. B. et al. Biomolecular condensates formed by designer minimalistic peptides. Nat. Commun. 14, 421 (2023).

28. Gabryelczyk, B. et al. Hydrogen bond guidance and aromatic stacking drive liquid-liquid phase separation of intrinsically disordered histidine-rich peptides. Nat. Commun. 10, 5465 (2019).

29. Abbas, M., Lipiński, W. P., Nakashima, K. K., Huck, W. T. S. & Spruijt, E. A short peptide synthon for liquid–liquid phase separation. Nat. Chem. 13, 1046–1054 (2021).

30. Ruan, Z., Li, S., Grigoropoulos, A., Amiri, H., Hillburg, S. L., Chen, H., Jayapurna, I., Jiang, T., Gu, Z., Alexander-Katz, A., Bustamante, C., Huang, H., & Xu, T. Population-based heteropolymer design to mimic protein mictures. Nature. 615, 251-258 (2023).

31. Pappas, C. G. et al. Dynamic peptide libraries for the discovery of supramolecular nano[34]materials. Nat. Nanotechnol. 11, 960–967 (2016).

32. Fan, Z., Sun, L., Huang, Y., Wang, Y. & Zhang, M. Bioinspired fluorescent dipeptide nanoparticles for targeted cancer cell imaging and real-time monitoring of drug release. Nat.

Nanotechnol. 11, 388–394 (2016).

33. Khemaissa, S., Sagan, S. & Walrant, A. 3.2. Hydrophobicity and Hydrophobic Effects - Tryptophan, an Amino-Acid Endowed with Unique Properties and Its Many Roles in Membrane. Crystals 11, 6 (2021).

34. Khemaissa, S., Walrant, A. & Sagan, S. Tryptophan, more than just an interfacial amino acid in the membrane activity of cationic cell-penetrating and antimicrobial peptides. Q. Rev. Biophys. 55, (2022).

35. Andersen, O. S., Greathouse, D. V., Providence, L. L., Becker, M. D. & Koeppe, R. E. Importance of tryptophan dipoles for protein function: F-fluorination of tryptophans in gramicidin a channels. J. Am. Chem. Soc. 120, 5142–5146 (1998).

36. Diaferia, C. et al. Structural Characterization of Self-Assembled Tetra-Tryptophan Based Nanostructures: Variations on a Common Theme. ChemPhysChem 19, 1635–1642 (2018).

37. Scheiner, S., Kar, T. & Pattanayak, J. Comparison of various types of hydrogen bonds involving aromatic amino acids. J. Am. Chem. Soc. 124, 13257–13264 (2002).

38. Moon, B. U. et al. Evaporation-Driven Water-in-Water Droplet Formation. Langmuir 36, 14333–14341 (2020).

39. Shaw, M., Bella, A. & Ryadnov, M. G. CREIM: Coffee ring effect imaging model for monitoring protein self-assembly in situ. J. Phys. Chem. Lett. 8, 4846–4851 (2017).

40. Cohen-gerassi, D. et al. Phase Transition and Crystallization Kinetics of a Supramolecular System in a Microfluidic Platform. ACS Publications. 32, 8342-8349 (2020).

41. Vivian, J. T. & Callis, P. R. Mechanisms of tryptophan fluorescence shifts in proteins. Biophys. J. 80, 2093–2109 (2001).

42. Kwok, A. et al. A Thermodynamic Model for Interpreting Tryptophan Excitation-Energy-Dependent Fluorescence Spectra Provides Insight Into Protein Conformational Sampling and Stability. Front. Mol. Biosci. 8, 1–13 (2021).

43. Liu, H., Zhang, H. & Jin, B. Fluorescence of tryptophan in aqueous solution. Spectrochim. Acta - Part A Mol. Biomol. Spectrosc. 106, 54–59 (2013).

44. Yang, H., Xiao, X., Zhao, X. & Wu, Y. Intrinsic Fluorescence Spectra of Tryptophan, Tyrosine and Phenyloalanine. Selected Papers of the Chinese Society for Optical Engineering Conferences held October and November 2016. 10255, 1199-1206 (2017).

45. Stollar, E. J. et al. Unconventional interactions between water and heterocyclic nitrogens

in protein structures. Proteins Struct. Funct. Genet. 57, 1–8 (2004).

46. Scott, G.G., McKnight, P.J., Tuttle, T. and Ulijn, R.V., Tripeptide Emulsifiers, Adv. Mater., 28, 1381-1386 (2016).

47. Maldonado-Valderrama, J., Wege, H. A., Rodríguez-Valverde, M. A., Gálvez-Ruiz, M. J. & Cabrerizo-Vílchez, M. A. Comparative study of adsorbed and spread β-casein monolayers at the water-air interface with the pendant drop technique. Langmuir 19, 8436–8442 (2003).

48. Kumar, M. et al. In situ, noncovalent labeling and stimulated emission depletion-based super-resolution imaging of supramolecular peptide nanostructures. ACS Nano 14, 15056–15063 (2020).

49. Brian Panganiban et al. Random heteropolymers preserve protein function in foreign environments. Science 359, 1239 – 1243 (2018).